Targeting the EphB4 Receptor for Cancer Diagnosis and Therapy Monitoring

ARTICLE *in* MOLECULAR PHARMACEUTICS · DECEMBER 2012

Impact Factor: 4.38 · DOI: 10.1021/mp300461b · Source: PubMed

10 AUTHORS, INCLUDING:

Shuanglong Liu
University of Southern California
69 PUBLICATIONS **1,552** CITATIONS
SEE PROFILE

Zibo Li
University of North Carolina at Chapel Hill
116 PUBLICATIONS **4,245** CITATIONS
SEE PROFILE

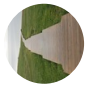

Hong Shan
Sun Yat-Sen University
125 PUBLICATIONS **754** CITATIONS
SEE PROFILE

Peter S Conti
University of Southern California
261 PUBLICATIONS **7,210** CITATIONS
SEE PROFILE

molecular pharmaceutics

Article

pubs.acs.org/molecularpharmaceutics

Targeting the EphB4 Receptor for Cancer Diagnosis and Therapy Monitoring

Dan Li,[†,‡] Shuanglong Liu,[†] Ren Liu,[§] Ryan Park,[†] Lindsey Hughes,[†] Valery Krasnoperov,[∥] Parkash S. Gill,[§] Zibo Li,[*,†] Hong Shan,[*,‡] and Peter S. Conti[†]

[†]Molecular Imaging Center, Department of Radiology, University of Southern California, Los Angeles, California 90033, United States

[‡]Department of Radiology, The Third Affiliated Hospital of Sun Yat-sen University, Guangzhou 510630, China

[§]Department of Pathology, University of Southern California, Los Angeles, California 90033, United States

[∥]Vasgene Therapeutics Inc., Los Angeles, California 90033, United States

ABSTRACT: Accumulating evidence suggests that EphB4 plays key roles in cancer progression in numerous cancer types. In fact, therapies focusing on EphB4 have become potentially important components of various cancer treatment strategies. However, tumor sensitivity to EphB4 suppression may not be uniform for different cancers. In this study, we developed near-infrared fluorescence (NIRF) probes for EphB4 targeted imaging, based on EphB4-specific humanized monoclonal antibody hAb47. NIRF dye Cy5.5 was introduced to hAb47 either through the reaction with amino groups (named hAb47-Cy5.5) or sulfhydryl groups (named hAb47-Cy5.5-Mal). The resulting probes were evaluated in both HT-29 xenograft and the mAb131 (anti-EphB4) treated models. Although these methods lead to modifications of both the heavy chain and light chain of the antibody, the majority of the EphB4 binding affinity was maintained (81.62 ± 2.08% for hAb47-Cy5.5 and 77.14 ± 2.46% for hAb47-Cy5.5-Mal, respectively). hAb47-Cy5.5 was then chosen for *in vivo* NIRF imaging of EphB4 expression. In HT29 colorectal tumor xenografts, hAb47-Cy5.5 demonstrated significantly higher tumor uptake compared with that of the hIgG-Cy5.5 control, which was further confirmed by immunofluorescent staining. Moreover, hAb47-Cy5.5 successfully imaged the decreased EphB4 expression (confirmed by Western blot) in EphB4-targeted immunotherapy using another EphB4-specific antibody, mAb131. Collectively, hAb47-Cy5.5 could be used as a specific NIRF contrast agent for noninvasive imaging of EphB4 expression, which may predict whether an individual tumor would likely respond to EphB4 targeted interventions, as well as monitor the therapeutic response.

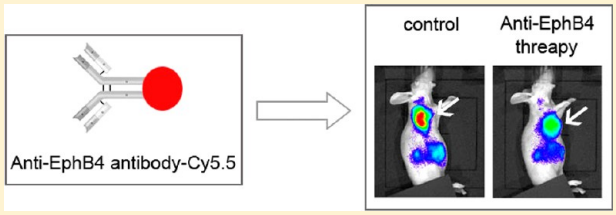

KEYWORDS: *EphB4 receptor, antibody, near-infrared fluorescence (NIRF) imaging, immunotherapy*

INTRODUCTION

The erythropoietin-producing hepatoma (Eph) receptors represent the largest class of receptor tyrosine kinases (RTKs) with 14 members. Ligands for Eph receptors are the membrane-bound Ephrins. Both Eph receptors and Ephrins are divided into two subgroups, A and B, based on sequence homologies and their binding affinities.[1] EphB4 and its sole ligand EphrinB2 play important roles in vascular remodeling of primitive capillary networks into distinct arteries and veins.[2,3] Human tumor tissue analysis has shown that EphB4 is profoundly up-regulated in numerous cancer types including prostate cancer, breast cancer, squamous cell carcinoma of the head and neck, bladder cancer, ovarian cancer, and colorectal cancer.[4−9] EphB4 directly supports tumorigenesis via forward signaling and angiogenesis via reverse signaling through EphrinB2 interaction.[10] Taking colorectal cancer, for example, EphB4 is absent in the normal colon but is expressed in all 102 colorectal cancer specimens analyzed.[9] A gain of EphB4 provides survival advantage to colorectal tumor cells, and EphB4 knockdown increases the sensitivity of tumor cells to tumor necrosis factor-related apoptosis-inducing ligand (TRAIL)-induced apoptosis.[9] On the basis of the extremely important function of EphB4, therapies focusing on EphB4 have become potentially important components of various cancer treatment strategies.[4−6,10−13] However, tumor sensitivity to EphB4 suppression will not be uniform for all cancer types, including primary versus metastatic disease. There is an urgent need to better predict which patients and individual tumors are likely to respond to such novel interventions as well as monitor the therapeutic response.

In order to meet the demand for the rapid development and clinical application of anti-EphB4 based cancer therapy, it is desirable to develop noninvasive imaging methods to visualize and quantify EphB4 suppression *in vivo*. Recently, EphB4-specific mouse-originated monoclonal antibodies have been

Received: August 21, 2012
Revised: November 3, 2012
Accepted: December 4, 2012
Published: December 4, 2012

developed to target the extracellular domain of EphB4, which did not recognize other members of the Eph family.[14] One of these antibodies, MAb47, binds to fibronectin-like domain 2 of both human and murine EphB4 with high affinity (kDa of 0.8 nmol/L). Humanized Ab47 (hAb47) was also developed for clinical application. In this study, we investigate whether hAb47 can be used for the noninvasive imaging of EphB4 on the colorectal cancer xenograft model after labeling with near-infrared fluorescence (NIRF) dyes. The probe was also applied to track the down-regulated EphB4 expression based on EphB4-targeted immunotherapy.

MATERIALS AND METHODS

Materials. All monoclonal anti-EphB4 antibodies (described bellow), EphB4-alkaline phosphatase (AP), and EphB4-human serum albumin (HSA) were kindly provided by Vasgene Therapeutics Inc. (Los Angeles, CA). hAb47 (humanized; recognizes both human and mouse EphB4) was used for probe synthesis and optical imaging, hAb131 (humanized; recognizes human EphB4) and rAb12D8 (rat origin; recognizes both human and mouse EphB4) for immunofluorescence, mAb131 (mouse origin; recognizes human EphB4) for therapy, and mAb265 (mouse origin; recognizes both human and mouse EphB4) for Western blot. Cy5.5 monofunctional *N*-hydroxysuccinimide ester (Cy5.5-NHS), Cy5.5-maleimide, and PD-10 disposable columns were purchased from GE Healthcare Life Sciences (NJ, USA), human IgG (hIgG), and mouse IgG (mIgG) from Rockland (Gilbertsville, PA), CD31 antibody from BD Pharmingen (San Diego, CA), β-Actin antibody from Sigma (St Louis, MO), and secondary antibodies goat antihuman Alexa Fluor 568 and goat antirat Alexa Fluor 488 from Invitrogen (Paisley, Scotland).

Synthesis of hAb47-Cy5.5, hAb47-Cy5.5-Mal, and hIgG-Cy5.5. An aqueous solution of hAb47 (500 μg) was mixed with Cy5.5-NHS in borate buffer at pH 8.5. The molar ratio of hAb47 to Cy5.5-NHS was 1:1. After stirring at room temperature for 1.5 h, the reaction mixture was passed through a gel filtration PD-10 column eluted with PBS solution. hIgG-Cy5.5 was also synthesized following the above-described procedures. To synthesize hAb47-Cy5.5-Mal, an aqueous solution of hAb47 (500 μg) was mixed with TCEP (100 mM, 5 μL) in PBS for 1 h. Cy5.5-Mal was then added to the mixture with a molar ratio of 1:1. After stirring at room temperature for 1.5 h, the reaction mixture was passed through a gel filtration PD-10 column eluted with PBS solution. The fluorescence intensity of hAb47-Cy5.5, hAb47-Cy5.5-Mal, and hIgG-Cy5.5 was evaluated by measuring the OD 680 nm with a Beckman DU 530 spectrophotometer (Beckman Instruments Inc., Fullerton, CA).

SDS–PAGE and Gel Infrared Imaging. hAb47, hAb47-Cy5.5, and hAb47-Cy5.5-Mal were mixed with Laemmli buffer (BioRad, Hercules, CA) containing 8 mg/mL dithiothreitol and heated at 100 °C for 5 min. Samples were fractionated on a 4% to 20% Tris-glycine gradient gel (Bio-Rad, Hercules, CA). Then, the gel was stained with Coomassie blue and scanned in both 700 nm and 800 nm channels with Odyssey Infrared Imager (LI-COR, Lincoln, NE).

Binding Activity Assay. The EphB4 binding activity of hIgG-Cy5.5, hAb47-Cy5.5, and hAb47-Cy5.5-Mal was evaluated through the bead-based binding assay with EphB4-alkaline phosphatase (AP). EphB4-AP (300 ng) was incubated with 50 ng of hIgG-Cy5.5, hAb47-Cy5.5, hAb47-Cy5.5-Mal, or hAb47 immobilized on Protein G-Agarose (5 μL/tube) for 1 h. Unbound proteins were removed by washing twice with PBS, and precipitated AP activity (OD405 value) was detected with *para*-nitro-phenylphosphate (PNPP). 0, 10, 20, 40, 80, and 120 ng of hAb47 were used as standards to get the standard curve and mathematical formula. OD405 values were set as X and quantities of hAb47 (ng) as Y. The active quantity (ng) of hIgG-Cy5.5, hAb47-Cy5.5, hAb47-Cy5.5-Mal, or hAb47 was then calculated according to the mathematical formula. Binding activity of hAb47-Cy5.5 = (ng of active hAb47-Cy5.5)/(ng of active hAb47). Biding activity of hIgG-Cy5.5 and hAb47-Cy5.5-Mal was calculated accordingly. Each sample was repeated in triplicate.

Binding Function Assay. EphB4-HSA was immobilized (500 ng/well) at 4 °C overnight on a 96-well plate. Wells were blocked with 0.5% BSA in PBS for 30 min at room temperature, followed by the application of hAb47-Cy5.5 or hIgG-Cy5.5 at different concentrations (5, 2.5, 1.25, 0.625, 0.313, 0.157, and 0.078 μg/mL) for 3 h at room temperature. Unbound proteins were removed by washing four times with PBS, and the fluorescence intensity of Cy5.5 was evaluated with Odyssey Infrared Imager (LI-COR, Lincoln, NE). Wells without the addition of EphB4-HSA served as negative controls.

Cell Culture. The human colorectal cancer cell line HT29 was obtained from American Type Culture Collection (Manassas, VA) and was maintained at 37 °C in a humidified atmosphere containing 5% CO_2 in RPMI-1640 and 10% fetal bovine serum (Omega Scientific, Tarzana, CA).

Tumor Xenografts. Animal procedures were performed according to the protocol approved by the University of Southern California Institutional Animal Care and Use Committee. Female athymic nude mice (BALB/c nu/nu), obtained from Harlan (Indianapolis, IN) at 4 to 6 weeks of age, were given injections subcutaneously in the right shoulder with 2×10^6 of HT29 human colorectal cancer cells suspended in100 μL of PBS.

***In Vivo* and *Ex Vivo* Near-Infrared Fluorescence (NIRF) Imaging.** *In vivo* fluorescence imaging was performed using the Xenogen Lumina XR Imaging System and analyzed using IVIS Living Imaging 3.0 software (Caliper Life Sciences, Alameda, CA). A Cy5.5 filter set was used for acquiring the fluorescence of Cy5.5-conjugated hAb47 or hIgG. Identical illumination settings (lamp voltage, filters, f/stop, field of views, and binning) were used for acquiring all images. Fluorescence emission images were normalized and reported as photons per second per centimeter squared per steradian (p/s/cm^2/sr). The mice were divided into two groups (n = 6 each group). The tumors of each group were size-matched. The mice of these two groups were injected via the tail vein with 30 μg of hAb47-Cy5.5 or hIgG-Cy5.5, and the animals underwent optical imaging at various time points after injection. Mice of these two groups were euthanized at 120 h postinjection (p.i.). The tumor and major organs were dissected and subjected to *ex vivo* fluorescence imaging. The mean fluorescence for each sample was reported.

mAb131 Therapy. The mice were divided into two groups (n = 6 each group). The tumors of each group were size-matched. One group was treated by peritoneal injection of mAb131 three times a week at a dose of 20 mg/kg. The control group was treated with the same dose of mIgG. After therapy, the mice of both groups were injected via the tail vein with 30 μg of hAb47-Cy5.5 for *in vivo* imaging at various time points and *ex vivo* imaging at 48 h p.i.

Immunofluorescence Staining. Tumors were dissected and embedded in Tissue-Tec optimal-cutting-temperature compound (Sakura Finetek, Torrance, CA). Frozen sections of tumors (5 μm) were fixed in 4% paraformaldehyde (Electron Microscopy Sciences, Hatfield, PA) and blocked with 10% normal goat serum (Invitrogen, Paisley, Scotland). Sections were then incubated with primary antibody overnight at 4 °C, followed by the corresponding secondary antibody for 1 h at room temperature. Subsequently, the slides were covered with VECTASHIELD Mounting Medium with DAPI (Burlingame, CA), and images were obtained with Nikon Eclipse 80i fluorescence microscope (Tokyo, Japan). Secondary antibody goat antihuman Alexa Fluor 568 was used to determine the localization and distribution of hAb47-Cy5.5 or hIgG-Cy5.5 in the tumor tissue after injection. It was also used to detect hAb131 primary antibody. Secondary antibody goat antirat Alexa Fluor 488 was used to detect CD31 and the rAb12D8 primary antibody.

Competition Binding Assay. The main purpose of the experiment is to detect whether mAb131 and mAb47 compete with each other for EphB4 binding. In detail, 5000 ng of nonbiotinylated mAb131 or mAb47 was preincubated with 500 ng of EphB4-AP for 1 h. The formed complex was added to streptavidin-Fe-Megnetic beads with 50 ng of immobilized biotinylated mAb47. After 1 h of incubation, unbound proteins were removed by washing twice with PBS. The precipitated AP activity was detected with *para*-nitro-phenylphosphate (PNPP). The EphB4 binding activity of hAb47 without the preincubation with nonbiotinylated antibodies was set as the control.

Western Blot. Proteins extracted from tumor tissue homogenate were resolved on 4% to 20% SDS−PAGE and transferred onto polyvinylidene difluoride membrane (Bio-Rad, Hercules, CA). Nonspecific binding was blocked with 5% nonfat dry milk in TBST (Tris-buffered saline with 0.1% Tween-20). Membranes were first probed with primary antibody overnight at 4 °C, washed, and probed with the secondary antibody for 1 h at room temperature, and developed.

Statistical Analysis. Quantitative data are expressed as the mean ± standard error of mean (SEM). Means were compared using one-way ANOVA and the Student's *t* test. *P* values of <0.05 were considered statistically significant.

RESULTS

Synthesis and Characterization of hAb47-Cy5.5, hAb47-Cy5.5-Mal, and hIgG-Cy5.5. hAb47 was conjugated with Cy5.5 through two methods. As shown in Figure 1A, each hAb47 molecule has four terminal amino groups and several lysine side chain amino groups available for conjugation with Cy5.5-NHS, which would lead to hAb47-Cy5.5. Alternatively, after partial reduction of disulfide bonds, sulfhydryl groups of hAb47 molecule are available for conjugation with Cy5.5-maleimide, which would result in hAb47-Cy5.5-Mal. In order to determine the Cy5.5 labeling sites of hAb47-Cy5.5 and hAb47-Cy5.5-Mal, these probes were fractionated by gel electrophoresis. The gel was stained with Coomassie blue and scanned in both 700 nm and 800 nm channels with Odyssey Infrared Imager. hAb47 can be stained with Coomassie blue. Coomassie blue-stained hAb47could be detected in both the 700 nm and 800 nm channels, while Cy5.5 could only be detected in the 700 nm channel. Figure 1B (shows the comparison between the 700 nm and 800 nm channels) clearly demonstrated that both the heavy chains and light chains of hAb47 were labeled with

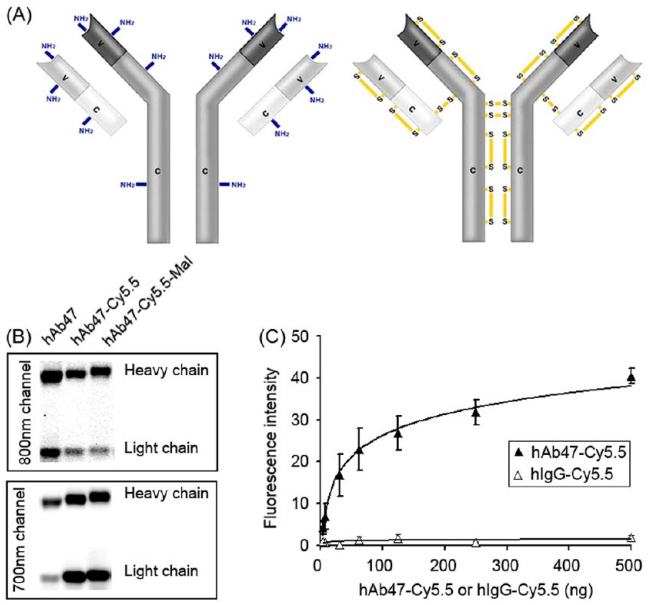

Figure 1. (A) Diagram of amino groups and sulfhydryl groups available for conjugation with Cy5.5-NHS or Cy5.5-maleimide, respectively. (B) Infrared imaging of hAb47, hAb47-Cy5.5, and hAb47-Cy5.5-Mal after fractionation by gel electrophoresis. (C) Saturation binding assay of hAb47-Cy5.5 and hIgG-Cy5.5 on EphB4-HSA.

Cy5.5. To study the impact of Cy5.5 conjugation on the EphB4 binding ability, binding activity assay was performed. After labeling, the binding activity of hIgG-Cy5.5, hAb47-Cy5.5, and hAb47-Cy5.5-Mal was determined to be (0.024 ± 0.07)%, (81.62 ± 2.08)%, and (77.14 ± 2.46)% of the untouched hAb47, respectively. Therefore, hAb47-Cy5.5, which possesses slightly higher binding activity, was chosen for further study. The binding specificity of hAb47-Cy5.5 to EphB4 was also determined through the saturation binding assay. As shown in Figure 1C, hAb47-Cy5.5 had binding function toward EphB4, while hIgG-Cy5.5 has minimal binding toward this target.

HT29 Tumor Tissue Analysis. We selected the HT29 colorectal tumor cell as the EphB4 positive tumor model. Immunofluorescence staining of HT29 tumor tissue (Figure 2) clearly demonstrated that HT29 tumor cells overexpress the EphB4 receptor, which correlated with literature reports.[9] Nests of tumor cells were surrounded by abundant stromal tissue containing neovasculature (CD31 positive), which could apply nutrition support on the one hand and deliver diagnostic or therapeutic probes to tumor cells on the other hand (Figure 2).

hAb47-Cy5.5 Demonstrated Prominent Uptake in HT29 Tumors. Mice bearing HT29 tumors (n = 6; EphB4 positive) were subjected to NIRF imaging at various time points postintravenous injection of hAb47-Cy5.5. hIgG-Cy5.5 was used as the control to validate the targeting specificity of the hAb47-Cy5.5. Figure 3A shows typical NIRF images of tumor-bearing mice administered with 30 μg of hAb47-Cy5.5 or hIgG-Cy5.5. In the mice administered with hAb47-Cy5.5, the tumor uptake was low at 6 h p.i., when the injected probe was still mainly in the blood pool. The uptake of hAb47-Cy5.5 into HT29 tumors was greatly increased and reached the plateau at 48 h p.i. To confirm the receptor specificity of hAb47-Cy5.5 *in vivo* and evaluate the active targeting effect, hIgG-Cy5.5 that does not bind to EphB4 was also tested. The uptake of hIgG-Cy5.5 into HT29 tumors was significantly

dx.doi.org/10.1021/mp300461b | *Mol. Pharmaceutics* 2013, 10, 329−336

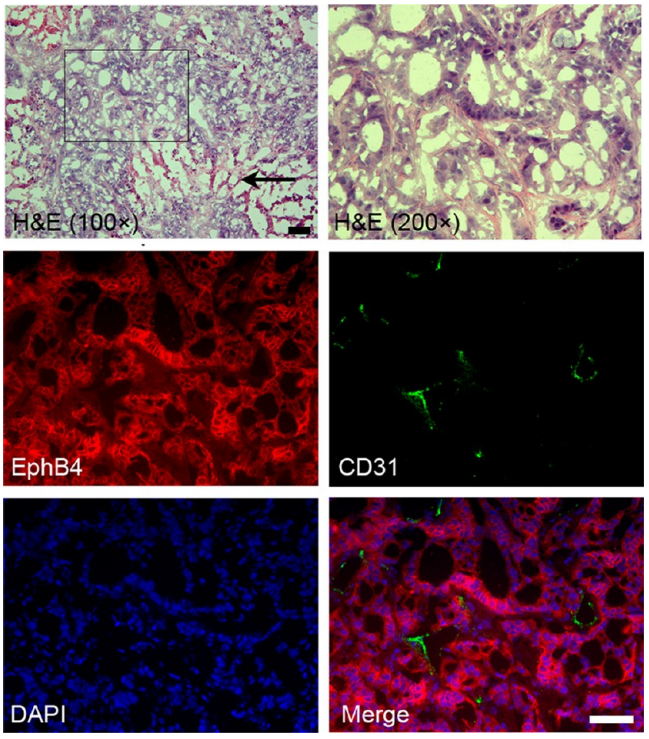

Figure 2. EphB4 and CD31 costaining on HT29 tumor sections. The black arrow indicates the necrosis area. Scale bar, 20 μm.

lower than that of hAb47-Cy5.5 at all time points examined ($P < 0.05$, Figure 3B). The tumor uptake of hIgG-Cy5.5 reached a plateau between 24 and 72 h followed by a steady decrease afterward. *Ex vivo* imaging was performed to validate the *in vivo* NIRF imaging data (120 h p.i.). As shown in Figure 3C,D, the tumor fluorescence intensity of mice administered with hAb47-Cy5.5 was 0.81 times higher than that of hIgG-Cy5.5, which was consistent with *in vivo* NIRF imaging results. The liver showed medium uptake of the two probes, mainly because the liver is responsible for the metabolism of high molecular weight antibodies.

Analysis of Probe Distribution Pattern in Tumor Tissues. To compare the distribution pattern of these two probes in HT29 tumor tissues, human secondary antibody was used to detect hAb47-Cy5.5 or hIgG-Cy5.5, while the CD31 antibody was used to visualize tumor vasculature. As the tumor uptake of the probes reached a plateau at 48 h p.i., tumor tissues were collected at this time point for the immunofluorescent assay. As shown in Figure 4, there was a large amount of hAb47 accumulated in the HT29 tumor tissues compared to hIgG, which was in accordance with the *in vivo* and *ex vivo* imaging results. Moreover, the hAb47 antibody was mainly found in tumor extravascular compartments at 48 h p.i., (Figure 4). All *in vivo*, *ex vivo*, and *in vitro* data supported the hypothesis that the high accumulation of hAb47-Cy5.5 over HT29 tumor region was due to the high expression of EphB4 among the tumors, which indicated that hAb47-Cy5.5 was capable of detecting EphB4 expression in a noninvasive mode.

hAb47-Cy5.5 Could Monitor the Efficacy of EphB4-Targeted Therapy on HT29 Tumors. Previously, it has been shown that mAb131 (an anti-EphB4 antibody) can reduce tumor growth through inducing endocytosis and degradation of EphB4.[14] To evaluate EphB4-targeted therapeutic efficacy, hAb47-Cy5.5 was administered to mAb131- or mIgG (control)-treated HT29 tumor-bearing mice. As shown in Figure 5A and B, the tumor uptake of hAb47-Cy5.5 decreased significantly at 24, 30, and 48 h in mAb131-treated mice compared to control mice ($P < 0.05$). *Ex vivo* images (Figure 5C,D) showed that the tumor fluorescence intensity of mAb131-treated mice was 0.74 times lower than that of control mice, which was consistent with *in vivo* NIRF imaging results. A competition binding assay was carried out to determine whether mAb131 and mAb47 compete with each other for EphB4 binding. As shown in Figure 5E, the binding of mAb47 toward EphB4 was not blocked even when mAb131 was incubated with EphB4 first. In contrast, the binding of

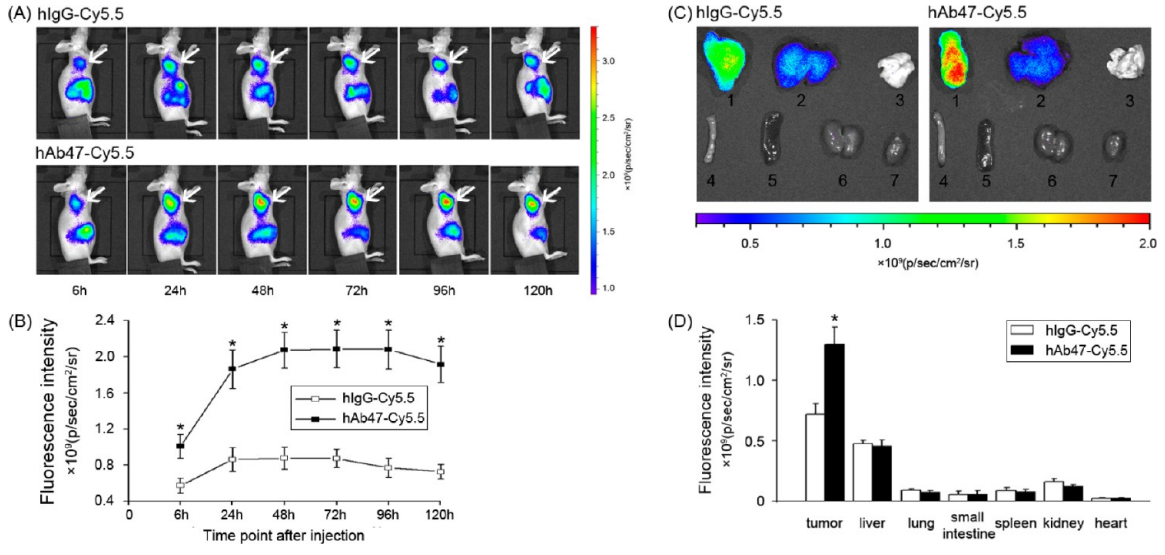

Figure 3. (A) *In vivo* near-infrared imaging of HT29 tumor-bearing mice after injection of hIgG-Cy5.5 or hAb47-Cy5.5 ($n = 6$ per group). The tumors are indicated by white arrows. (B) Time-fluorescence intensity curves of HT29 tumor for hIgG-Cy5.5 and hAb47-Cy5.5. (C) *Ex vivo* near-infrared imaging of major organs harvested at 120 h p.i. of hIgG-Cy5.5 or hAb47-Cy5.5. 1 tumor, 2 livers, 3 lungs, 4 small intestines, 5 spleens, 6 kidneys, and 7 hearts. (D) Fluorescence intensity quantification of tumors and major organs at 120 h p.i. of hIgG-Cy5.5 or hAb47-Cy5.5 respectively. All data in B and D are presented as the mean ± standard error of mean (SEM). The P value was calculated with Student's t test. *, $P < 0.05$.

dx.doi.org/10.1021/mp300461b | *Mol. Pharmaceutics* 2013, 10, 329–336

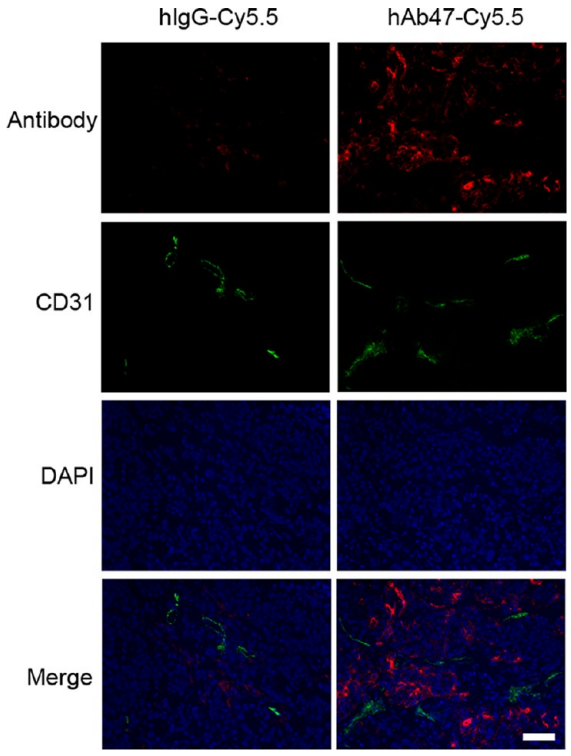

Figure 4. Antibody and CD31 costaining on HT29 tumor sections 48 h p.i. of hIgG-Cy5.5 or hAb47-Cy5.5, respectively. Scale bar, 20 μm.

mAb47 could be successfully blocked by mAb47. In order to confirm whether the reduced uptake was caused by decreased EphB4 expression, Western blot analysis of mAb131-treated and mIgG (control)-treated tumors was performed. As shown in Figure 6A, the tumor EphB4 level was markedly reduced in mAb131-treated mice compared to that in control mice. Immunofluorescence staining analysis indicated that lower distribution of hAb47 was accompanied by the loss of EphB4 in tumors treated with mAb131 (Figure 6B).

DISCUSSION

Accumulating evidence suggests that EphB4 is overexpressed in numerous cancer types and plays important roles in cancer progression and angiogenesis.[4−9] Therefore, EphB4 has become a novel target for cancer diagnosis and therapy. The ability to image EphB4 *in vivo* could be valuable for the evaluation of patients with a variety of malignancies, particularly for monitoring those therapies designed to block EphB4 function. Through EphB4-targeted molecular imaging, the expression level of EphB4 can be assessed noninvasively, and changes in EphB4 expression during treatment can be monitored. These would markedly aid in early and sensitive lesion detection, prognostic evaluation, patient selection for entering clinical trials, better treatment monitoring and dose optimization, and elucidation of the mechanisms of treatment efficacy underlying the relevant signaling pathways.[15]

Previously, peptide based probes have been developed for EphB4 targeted imaging, and promising results have been obtained.[16,17] However, both absolute tumor uptake and the pharmacokinetics of these probes need to be further improved. Antibodies are considered as potentially the most specific probes for imaging because they offer unmatched ability for selective binding to any target.[18] Recently, anti-EphB4 antibodies have been obtained for EphB4 binding with 1 nM affinity. The antibody has much higher EphB4 binding affinity and specificity compared with small peptides, which may lead to increased tumor uptake and improved distribution pattern. In this study, we developed a near-infrared (NIRF) fluorescence probe for EphB4 imaging, based on the EphB4-specific monoclonal antibody hAb47.[14] Moreover, the antibody based imaging probes would be more suitable for patient screening as they are closely related to the antibody drug to be used in the immunotherapy clinical trials.

In the initial study, hAb47 was conjugated with Cy5.5 through two different methods at a molar ratio of 1:1. (1) Amino group: Both the heavy chains and light chains of the antibody molecule have terminal amino groups; several lysine side chain amino groups are also available for conjugation with Cy5.5-NHS. (2) Sulfhydryl groups: After partial reduction of disulfide bonds, sulfhydryl groups on both the heavy chains and light chains of the antibody molecule are available for conjugation with Cy5.5-maleimide. After conjugation and purification, the gel infrared imaging results confirmed that both the heavy chains and light chains of hAb47 were labeled with Cy5.5 through these two methods (Figure 1B). Performing the conjugation at a molar ratio of 1:1 only slightly reduced the binding activity of hAb47 toward EphB4. Because there are several lysine side chain amino groups on both VH (variable region of the heavy chain) and VL (variable region of the light chain) of hAb47, the reduced binding ability of hAb47-Cy5.5 may be caused by the random conjugation of Cy5.5 at the site of VH or VL. Modification through the sulfhydryl group could be an alternative approach. Each IgG antibody molecule contains a total of 16 disulfide bonds including 4 interchain disulfide bonds in the hinge region and 12 intrachain disulfide bonds associated with 12 individual domains (see Figure 1A). Interchain disulfide bonds are more susceptible to reduction than intrachain disulfide bonds.[19] In addition, the disulfide bonds between the light chain and heavy chain are more susceptible than disulfide bonds between the two heavy chains.[19] Therefore, the partial reduction may lead to the separation of the single light chain from the heavy chain. The VH and VL together form the dimeric antigen-binding pocket. Some studies showed that the single light chain or single heavy chain fragments lost their antigen binding affinity.[20] This may explain the lower binding activity of hAb47-Cy5.5-Mal (77.14 ± 2.46%). As we did not observe a significant advantage with hAb47-Cy5.5-Mal, hAb47-Cy5.5 was used in further studies. In fact, the 1:1 Cy5.5/hAb reaction ratio gave a relatively high immuno-active fraction of the resulting Cy5.5-NHS labeled hAb47 because of fewer disturbances on the antigen binding domain. The binding specificity of hAb47-Cy5.5 to EphB4 was further confirmed through a saturation binding assay (Figure 1C).

After characterizing hAb47-Cy5.5 *in vitro*, we further tested this probe in HT29 tumor model. The Cy5.5 tag allowed its application in near-infrared (NIRF) fluorescence imaging. The enhanced permeability and retention (EPR) effect (due to the leaky vasculature and lack of lymphatic drain in the tumor) causes passive uptake of the macromolecule, such as antibodies, in the tumor.[21] In order to measure the specific targeting attributed to antibodies (antigen interaction causes active uptake of antibodies), hIgG-Cy5.5 was used as the control to evaluate the EPR effect. The tumor uptake of hIgG-Cy5.5 was comparatively low at all time points examined (Figure 3A,B). In contrast, the tumor uptake of hAb47-Cy5.5 increased with time and reached a plateau at 48 h (Figure 3A,B), which implied that

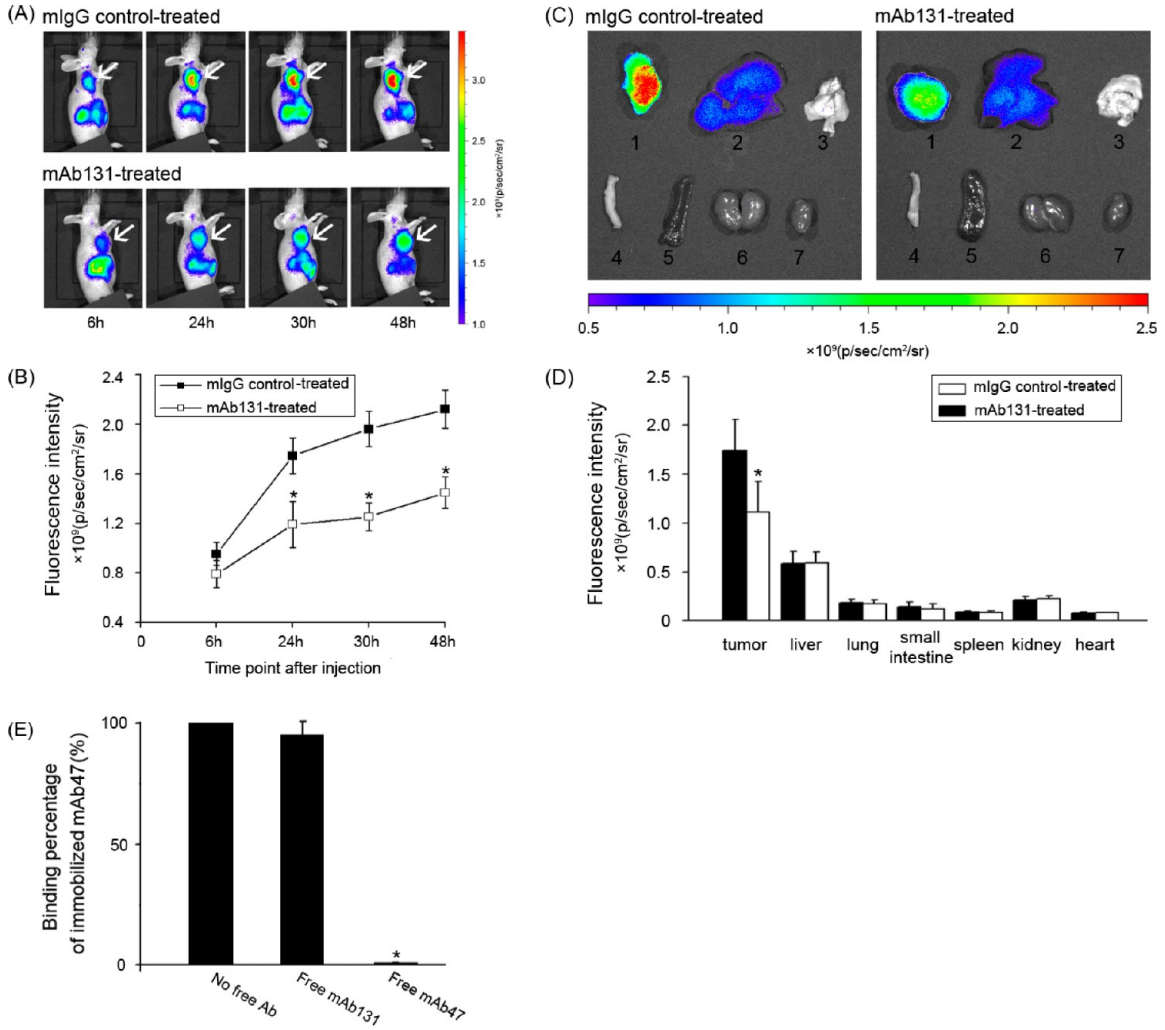

Figure 5. (A) In vivo near-infrared imaging of mAb131 or mIgG (control)-treated HT29 tumor-bearing mice after injection of hAb47-Cy5.5 (n = 6 per group). The tumors are indicated by white arrows. (B) Time-fluorescence intensity curves of HT29 tumor for hAb47-Cy5.5 of each group mice. (C) *Ex vivo* near-infrared imaging of major organs of mAb131 or mIgG (control)-treated HT29 tumor-bearing mice harvested at 48 h p.i. of hAb47-Cy5.5. 1 tumor, 2 livers, 3 lungs, 4 small intestines, 5 spleens, 6 kidneys, and 7 hearts. (D) Fluorescence intensity quantification of tumors and major organs of each group mice at 48 h p.i. of hAb47-Cy5.5. (E) Binding percentage of immobilized mAb47 to EphB4 when free mAb131, free mAb47, or no free antibodies were preincubated with EphB4-AP. All data in B and D were presented as the mean ± standard error of the mean (SEM). The P value was calculated with Student's t test. *, $P < 0.05$.

both the EPR effect and hAb47−EphB4 interaction contributed to the tumor uptake of hAb47-Cy5.5. *In vivo* imaging results were further confirmed by *ex vivo* imaging (Figure 3C,D) and immunofluorescent staining analysis (Figure 4). A previous study also showed that mAb47-Cy5 could bind to HT29 cells, while IgG-Cy5 could not,[14] which correlated well with the *in vivo* imaging results. The liver only showed a modest uptake of the two probes (Figure 3C,D), which could be caused by the Fc receptor in the liver and the native clearance route for high molecular weight antibodies (150 kDa). Although hAb47-Cy5.5 distributed only in HT29 tumor extravascular compartments at 48 h p.i. (Figure 4), EphB4 expression was detected on neovasculatures of some breast cancers and brain cancers, presumably of venous lineage.[5,22] Therefore, hAb47-Cy5.5 (also recognizes mouse EphB4) may be used to target EphB4 expressed on neovasculatures in these mouse models.

Overexpression of EphB4 has been discovered in various cancer cells. This receptor appears to function as a survival factor in various cancers and is a novel target for therapy.[4−6,10−13] In fact, inhibition of EphB4 expression could lead to decreased tumor cell viability, migration, invasion,[5−9] and sensitization of cancer cells to endogenous TRAIL[5,6,9] and chemotherapy.[23] Thus, noninvasively monitoring the expression level of EphB4 during the treatment process could aid in evaluating therapeutic efficacy and guiding therapy. mAb131 (binds to the fibronectin-like domain 1 of EphB4) has been shown to exert anticancer activities through inducing endocytosis and degradation of EphB4.[14] In contrast, mAb47 binds to fibronectin-like domain 2 of EphB4, which has minimal binding competition with mAb131 (Figure 5E). Therefore, hAb47-Cy5.5 was further applied to evaluate the changes of EphB4 expression level after mAb131 therapy. At late time points (24, 30, and 48 h), the tumor uptake of hAb47-Cy5.5 decreased significantly ($P < 0.05$) in mAb131-treated mice compared to that in the control (mIgG-treated) mice (Figure 5A,B). This result suggested that the EphB4-specific uptake of hAb47-Cy5.5 was depleted, and passive targeting may play a major role here. The reduction of EphB4 expression level in mAb131-treated HT29 tumors was further confirmed through Western blot and immunofluorescent staining analysis.

dx.doi.org/10.1021/mp300461b | *Mol. Pharmaceutics* 2013, 10, 329−336

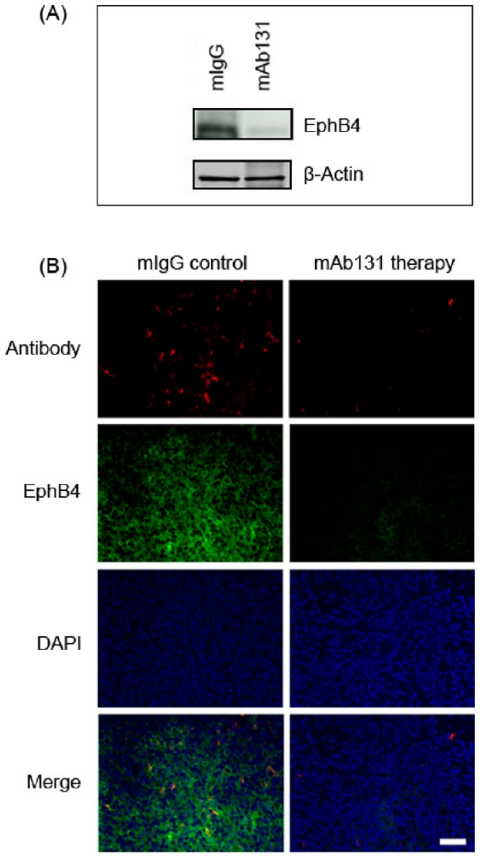

Figure 6. (A) Western blot analysis of EphB4 level in HT29 tumor tissues after mAb131 or mIgG (control) treatment. (B) Antibody and EphB4 costaining on tumor sections of mAb131 or mIgG (control)-treated HT29 tumor-bearing mice 48 h p.i. of hAb47-Cy5.5. Scale bar, 20 μm.

Immunofluorescent staining analysis also showed less distributed hAb47 in mAb131-treated HT29 tumors compared to that in the control due to the absence of EphB4 receptor.

Despite the success of this proof-of-principle optical imaging study in small animal models, there are also barriers to overcome before translating this hAb47-based imaging agent into clinical practice. The major disadvantage of optical imaging is the limited depth penetration and intense light scattering, which allows only for demarcation of superficial tumors and tissues accessible by endoscopy, as well as intraoperative imaging.[24] To obtain quantitative information about tumor targeting and distribution patterns of this imaging agent, positron emission tomography (PET) or single photon emission computed tomography (SPECT) will be required for further studies. Moreover, due to the large size (150 kDa) of antibodies, the intact immunoglobulins have slow tumor penetration and take longer time to optimally accrete in tumors (1−2 days).[25] Besides intact antibody molecules (molecular weight, ∼150 kDa), advancement in antibody engineering has led to the development of various forms of antibodies, such as $F(ab')_2$, F(ab′), single chain Fv (scFv), and the covalent dimers $scFv_2$, diabodies, and minibodies (molecular weights ranging from 25 to 100 kDa),[18,26] as well as several types of antibodies based on nontraditional scaffolds, for example, domain antibodies, affibodies, nanobodies, and anticalins.[27] Therefore, imaging studies based on antibodies with better pharmacokinetics are expected in the near future.

AUTHOR INFORMATION

Corresponding Author

*(Z.L.) Tel: 1-323-442-3557. Fax: 1-323-442-3253. E-mail: ziboli@usc.edu. (H.S.) Tel/Fax: +86-20-85252573. E-mail: shanhong@mail.sysu.edu.cn.

Notes

The authors declare the following competing financial interest(s): V.K. is the employee of Vasgene Therapeutics Inc.

ACKNOWLEDGMENTS

This work was supported by the NIBIB (R21 1 r21 eb012294-01a1), Early (Margaret E.) Medical Research Trust, the American Cancer Society (121991-MRSG-12-034-01-CCE), National Natural Science Foundation of China (No. U1032002, 81071206), and Key Clinical Research Project of Public Health Ministry of China 2010-2012 (No. 164).

REFERENCES

(1) Pasquale, E. B. Eph receptor signalling casts a wide net on cell behaviour. *Nat. Rev. Mol. Cell Biol.* **2005**, *6*, 462−475.

(2) Wang, H. U.; Chen, Z. F.; Anderson, D. J. Molecular distinction and angiogenic interaction between embryonic arteries and veins revealed by ephrin-B2 and its receptor Eph-B4. *Cell* **1998**, *93*, 741−753.

(3) Gerety, S. S.; Wang, H. U.; Chen, Z. F.; Anderson, D. J. Symmetrical mutant phenotypes of the receptor EphB4 and its specific transmembrane ligand ephrin-B2 in cardiovascular development. *Mol. Cell* **1999**, *4*, 403−414.

(4) Xia, G.; Kumar, S. R.; Masood, R.; Zhu, S.; Reddy, R.; Krasnoperov, V.; Quinn, D. I.; Henshall, S. M.; Sutherland, R. L.; Pinski, J. K.; Daneshmand, S.; Buscarini, M.; Stein, J. P.; Zhong, C.; Broek, D.; Roy-Burman, P.; Gill, P. S. EphB4 expression and biological significance in prostate cancer. *Cancer Res.* **2005**, *65*, 4623−4632.

(5) Kumar, S. R.; Singh, J.; Xia, G.; Krasnoperov, V.; Hassanieh, L.; Ley, E. J.; Scehnet, J.; Kumar, N. G.; Hawes, D.; Press, M. F.; Weaver, F. A.; Gill, P. S. Receptor tyrosine kinase EphB4 is a survival factor in breast cancer. *Am. J. Pathol.* **2006**, *169*, 279−293.

(6) Masood, R.; Kumar, S. R.; Sinha, U. K.; Crowe, D. L.; Krasnoperov, V.; Reddy, R. K.; Zozulya, S.; Singh, J.; Xia, G.; Broek, D.; Schonthal, A. H.; Gill, P. S. EphB4 provides survival advantage to squamous cell carcinoma of the head and neck. *Int. J. Cancer* **2006**, *119*, 1236−1248.

(7) Xia, G.; Kumar, S. R.; Stein, J. P.; Singh, J.; Krasnoperov, V.; Zhu, S.; Hassanieh, L.; Smith, D. L.; Buscarini, M.; Broek, D.; Quinn, D. I.; Weaver, F. A.; Gill, P. S. EphB4 receptor tyrosine kinase is expressed in bladder cancer and provides signals for cell survival. *Oncogene* **2006**, *25*, 769−780.

(8) Kumar, S. R.; Masood, R.; Spannuth, W. A.; Singh, J.; Scehnet, J.; Kleiber, G.; Jennings, N.; Deavers, M.; Krasnoperov, V.; Dubeau, L.; Weaver, F. A.; Sood, A. K.; Gill, P. S. The receptor tyrosine kinase EphB4 is overexpressed in ovarian cancer, provides survival signals and predicts poor outcome. *Br. J. Cancer* **2007**, *96*, 1083−1091.

(9) Kumar, S. R.; Scehnet, J. S.; Ley, E. J.; Singh, J.; Krasnoperov, V.; Liu, R.; Manchanda, P. K.; Ladner, R. D.; Hawes, D.; Weaver, F. A.; Beart, R. W.; Singh, G.; Nguyen, C.; Kahn, M.; Gill, P. S. Preferential induction of EphB4 over EphB2 and its implication in colorectal cancer progression. *Cancer Res.* **2009**, *69*, 3736−3745.

(10) Noren, N. K.; Pasquale, E. B. Paradoxes of the EphB4 receptor in cancer. *Cancer Res.* **2007**, *67*, 3994−3997.

(11) Berardi, A. C.; Marsilio, S.; Rofani, C.; Salvucci, O.; Altavista, P.; Perla, F. M.; Diomedi-Camassei, F.; Uccini, S.; Kokai, G.; Landuzzi, L.; McDowell, H. P.; Dominici, C. Up-regulation of EphB and ephrin-B expression in rhabdomyosarcoma. *Anticancer Res.* **2008**, *28*, 763−769.

(12) Yavrouian, E. J.; Sinha, U. K.; Rice, D. H.; Salam, M. T.; Gill, P. S.; Masood, R. The significance of EphB4 and EphrinB2 expression and survival in head and neck squamous cell carcinoma. *Arch. Otolaryngol. Head Neck Surg.* **2008**, *134*, 985−991.

(13) Zhang, S.; Jiang, T.; Liang, M. Expression of Eph B4 and Ephrin B2 in cervical cancer tissues and angiogenesis. *Int. J. Gynaecol. Obstet.* **2007**, *96*, 46−47.
(14) Krasnoperov, V.; Kumar, S. R.; Ley, E.; Li, X.; Scehnet, J.; Liu, R.; Zozulya, S.; Gill, P. S. Novel EphB4 monoclonal antibodies modulate angiogenesis and inhibit tumor growth. *Am. J. Pathol.* **2010**, *176*, 2029−2038.
(15) Cai, W.; Rao, J.; Gambhir, S. S.; Chen, X. How molecular imaging is speeding up antiangiogenic drug development. *Mol. Cancer Ther.* **2006**, *5*, 2624−2633.
(16) Xiong, C.; Huang, M.; Zhang, R.; Song, S.; Lu, W.; Flores, L., 2nd; Gelovani, J.; Li, C. In vivo small-animal PET/CT of EphB4 receptors using 64Cu-labeled peptide. *J. Nucl. Med.* **2011**, *52*, 241−248.
(17) Zhang, R.; Xiong, C.; Huang, M.; Zhou, M.; Huang, Q.; Wen, X.; Liang, D.; Li, C. Peptide-conjugated polymeric micellar nanoparticles for Dual SPECT and optical imaging of EphB4 receptors in prostate cancer xenografts. *Biomaterials* **2011**, *32*, 5872−5879.
(18) Kaur, S.; Venktaraman, G.; Jain, M.; Senapati, S.; Garg, P. K.; Batra, S. K. Recent trends in antibody-based oncologic imaging. *Cancer Lett.* **2012**, *315*, 97−111.
(19) Liu, H.; Chumsae, C.; Gaza-Bulseco, G.; Hurkmans, K.; Radziejewski, C. H. Ranking the susceptibility of disulfide bonds in human IgG1 antibodies by reduction, differential alkylation, and LC-MS analysis. *Anal. Chem.* **2010**, *82*, 5219−5226.
(20) Hu, C. M.; Kaushal, S.; Tran Cao, H. S.; Aryal, S.; Sartor, M.; Esener, S.; Bouvet, M.; Zhang, L. Half-antibody functionalized lipid-polymer hybrid nanoparticles for targeted drug delivery to carcinoembryonic antigen presenting pancreatic cancer cells. *Mol. Pharmaceutics* **2010**, *7*, 914−920.
(21) Maeda, H.; Wu, J.; Sawa, T.; Matsumura, Y.; Hori, K. Tumor vascular permeability and the EPR effect in macromolecular therapeutics: a review. *J. Controlled Release* **2000**, *65*, 271−284.
(22) Erber, R.; Eichelsbacher, U.; Powajbo, V.; Korn, T.; Djonov, V.; Lin, J.; Hammes, H. P.; Grobholz, R.; Ullrich, A.; Vajkoczy, P. EphB4 controls blood vascular morphogenesis during postnatal angiogenesis. *EMBO J.* **2006**, *25*, 628−641.
(23) Spannuth, W. A.; Mangala, L. S.; Stone, R. L.; Carroll, A. R.; Nishimura, M.; Shahzad, M. M.; Lee, S. J.; Moreno-Smith, M.; Nick, A. M.; Liu, R.; Jennings, N. B.; Lin, Y. G.; Merritt, W. M.; Coleman, R. L.; Vivas-Mejia, P. E.; Zhou, Y.; Krasnoperov, V.; Lopez-Berestein, G.; Gill, P. S.; Sood, A. K. Converging evidence for efficacy from parallel EphB4-targeted approaches in ovarian carcinoma. *Mol. Cancer Ther.* **2010**, *9*, 2377−2388.
(24) van Dam, G. M.; Themelis, G.; Crane, L. M.; Harlaar, N. J.; Pleijhuis, R. G.; Kelder, W.; Sarantopoulos, A.; de Jong, J. S.; Arts, H. J.; van der Zee, A. G.; Bart, J.; Low, P. S.; Ntziachristos, V. Intraoperative tumor-specific fluorescence imaging in ovarian cancer by folate receptor-alpha targeting: first in-human results. *Nat. Med.* **2011**, *17*, 1315−1319.
(25) Kelloff, G. J.; Krohn, K. A.; Larson, S. M.; Weissleder, R.; Mankoff, D. A.; Hoffman, J. M.; Link, J. M.; Guyton, K. Z.; Eckelman, W. C.; Scher, H. I.; O'Shaughnessy, J.; Cheson, B. D.; Sigman, C. C.; Tatum, J. L.; Mills, G. Q.; Sullivan, D. C.; Woodcock, J. The progress and promise of molecular imaging probes in oncologic drug development. *Clin. Cancer Res.* **2005**, *11*, 7967−7985.
(26) Holliger, P.; Hudson, P. J. Engineered antibody fragments and the rise of single domains. *Nat. Biotechnol.* **2005**, *23*, 1126−1136.
(27) Sheridan, C. Pharma consolidates its grip on post-antibody landscape. *Nat. Biotechnol.* **2007**, *25*, 365−366.